



TECHNISCHE UNIVERSITÄT
CHEMNITZ

Charakterisierung von Oberflächen

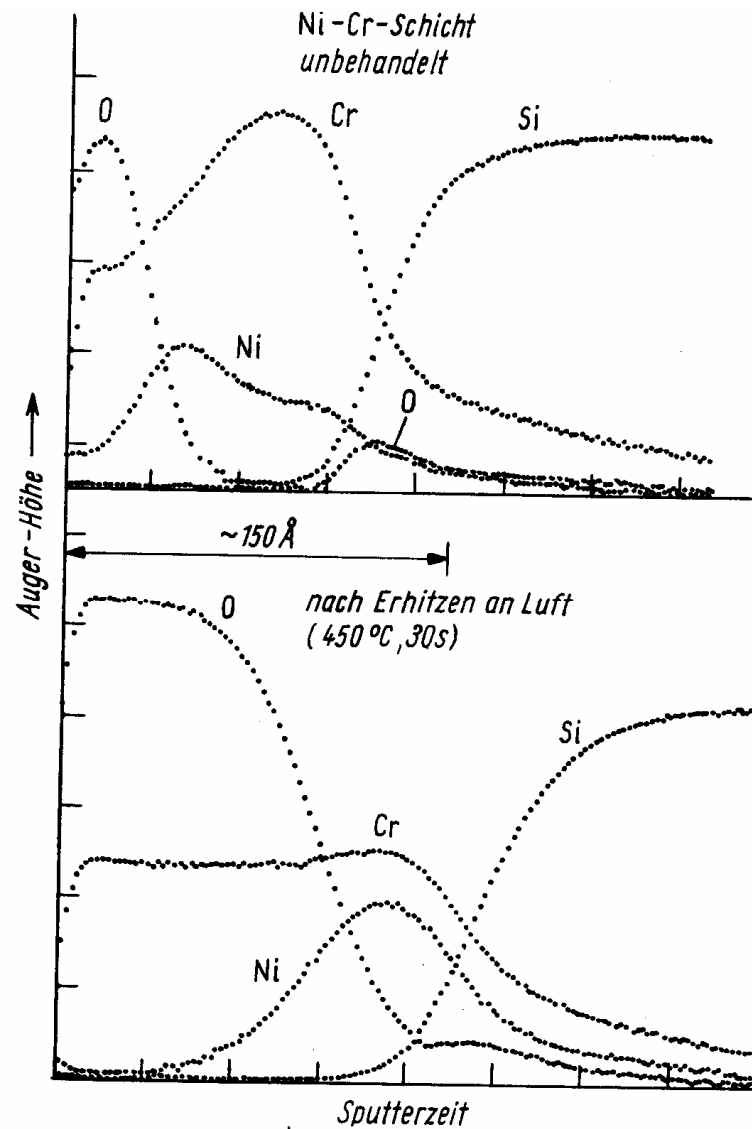
Rudolf Holze

Technische Universität Chemnitz, Institut für Chemie, AG Elektrochemie,
D-09107 Chemnitz, Germany





1. Einführung, Organisatorisches
2. Grundlagen, Gegenstand der Vorlesung
 - 2.1. Oberflächeneigenschaften: An den Grenzen fester Materie
 - 2.2. Übersicht über die wichtigsten Sonden und Signale, Wechselwirkungen und darauf basierende Methoden
3. Atomspektroskopie
 - 3.1. Augerelektronenspektroskopie
 - 3.2. Photoelektronenspektroskopie, XPS, UPS
4. Schwingungsspektroskopie
 - 4.1 EELS
 - 4.2 IR
 - 4.3 Raman-Spektroskopie
5. Ionenmethoden
 - 5.1. Sekundärionenmassenspektroskopie
 - 5.2. Thermodesorptions-MS, Laserdesorptions-MS
6. Elektronenstrahlmikroanalyse
7. Mößbauerspektroskopie
8. Elektrochemische Verfahren
 - 8.1 Klassische Verfahren
 - 8.2 Nichtklassische *ex situ*-Verfahren
 - 8.3 Nichtklassische *in situ*-Verfahren
9. BET, Mikro-Meso-Makroporen, Langmuir
10. Beispiele angewandter Methodenvielfalt:
 - 10.1. Heterogene Katalyse
 - 10.2. Korrosion



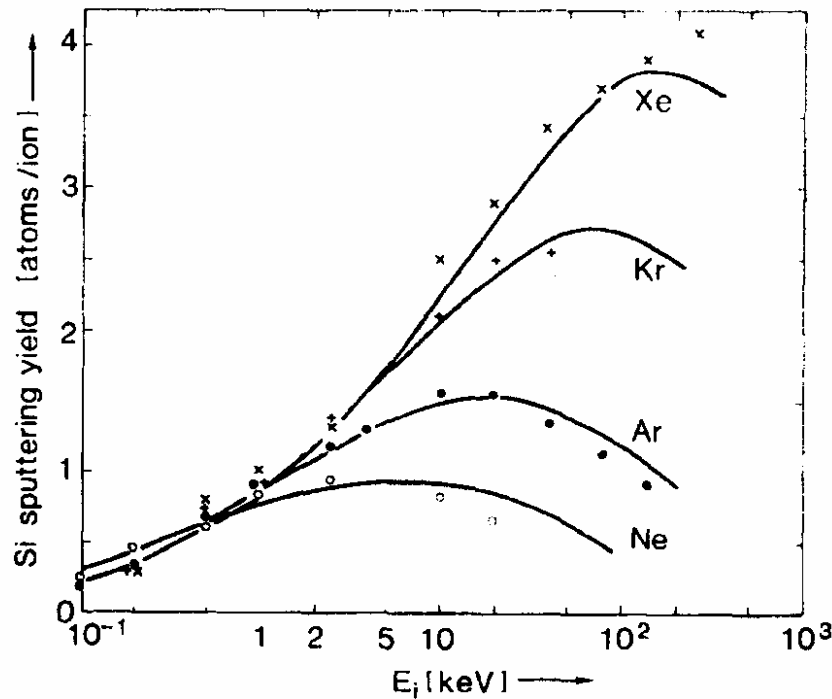
Tiefenprofile einer Nickel-Chrom-Schicht vor und nach dem Erhitzen an Luft (nach PALMBERG /5.6/)



5. Ionenmethoden

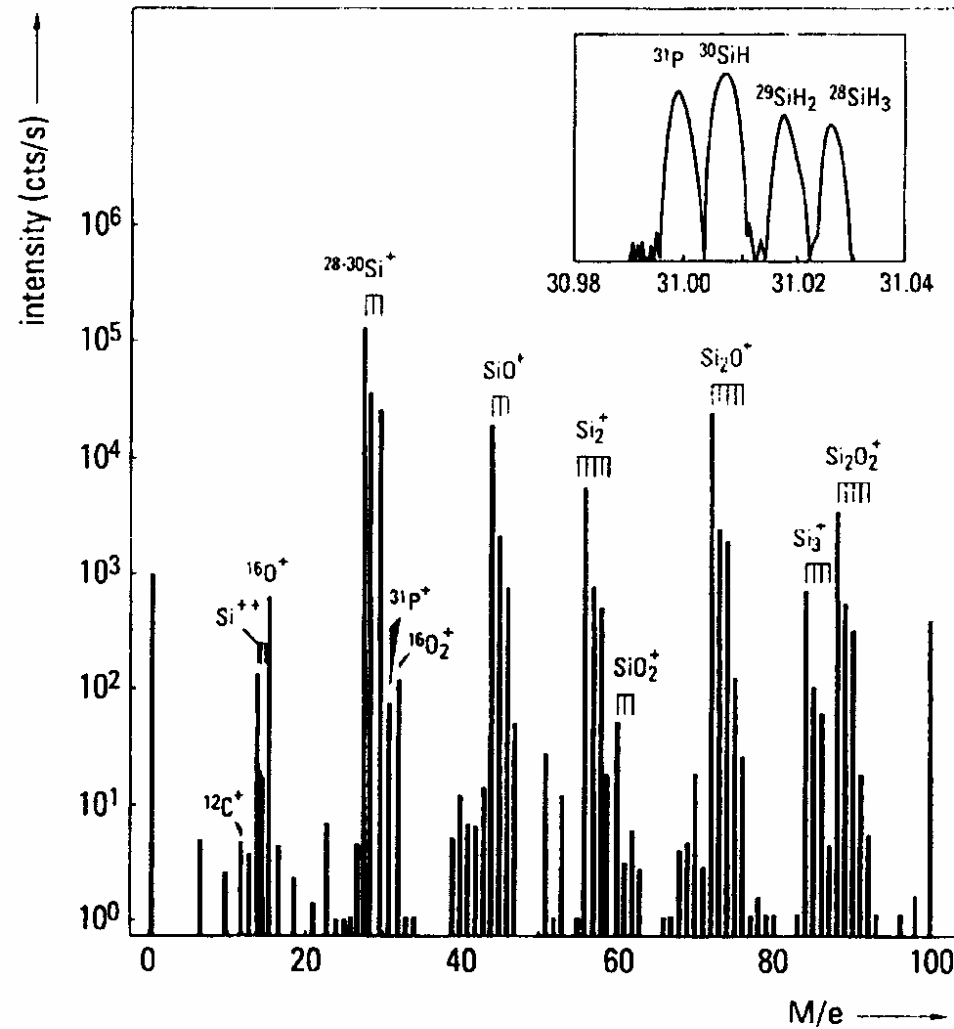
5.1. Sekundärionenmassenspektroskopie (SIMS)

5.2. Thermodesorptions-MS, Laserdesorptions-MS

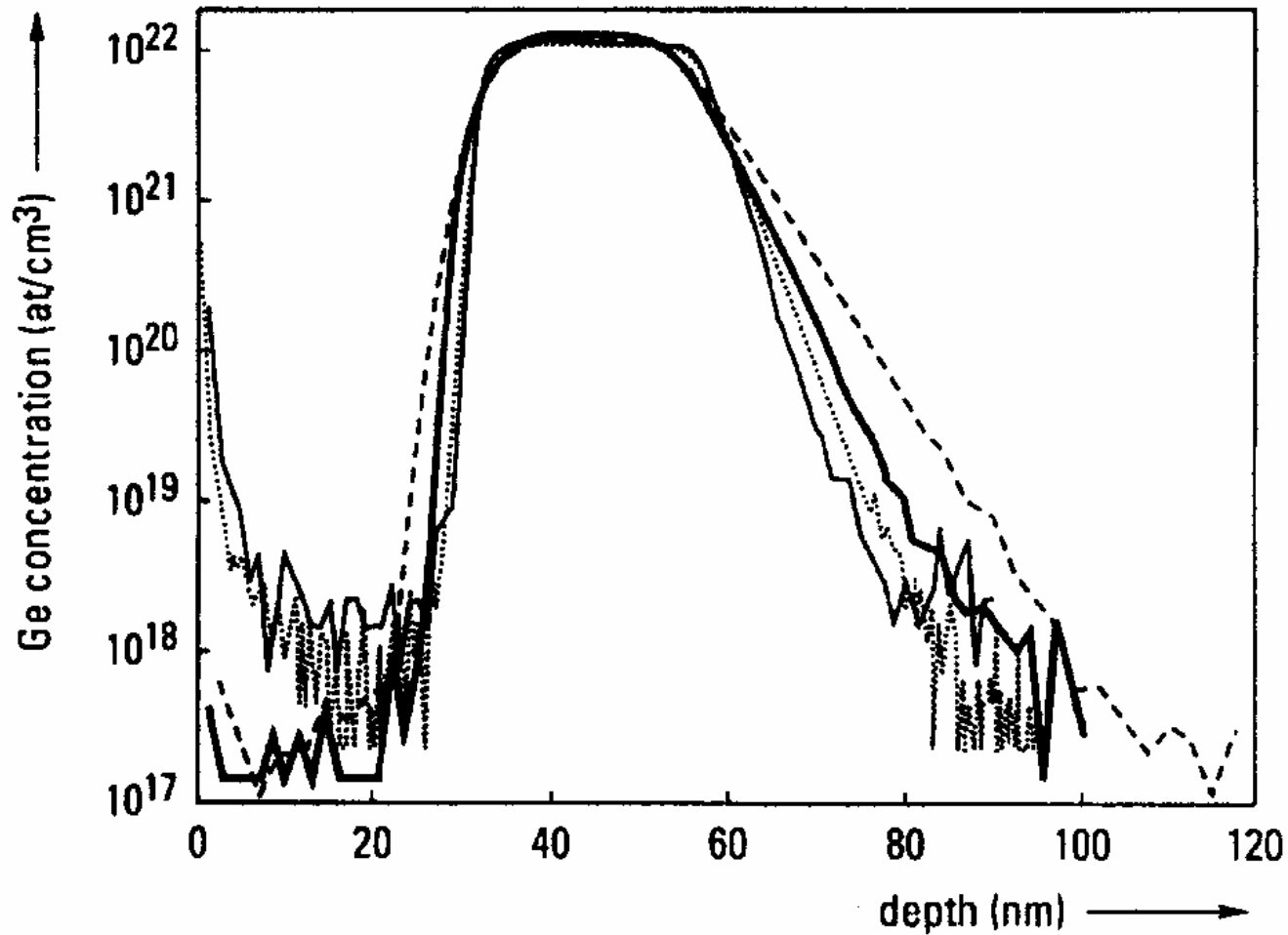


Energy dependence of the total sputtering yield for silicon bombarded with various noble gas ions at perpendicular incidence. The full lines are the predictions of equation (1).

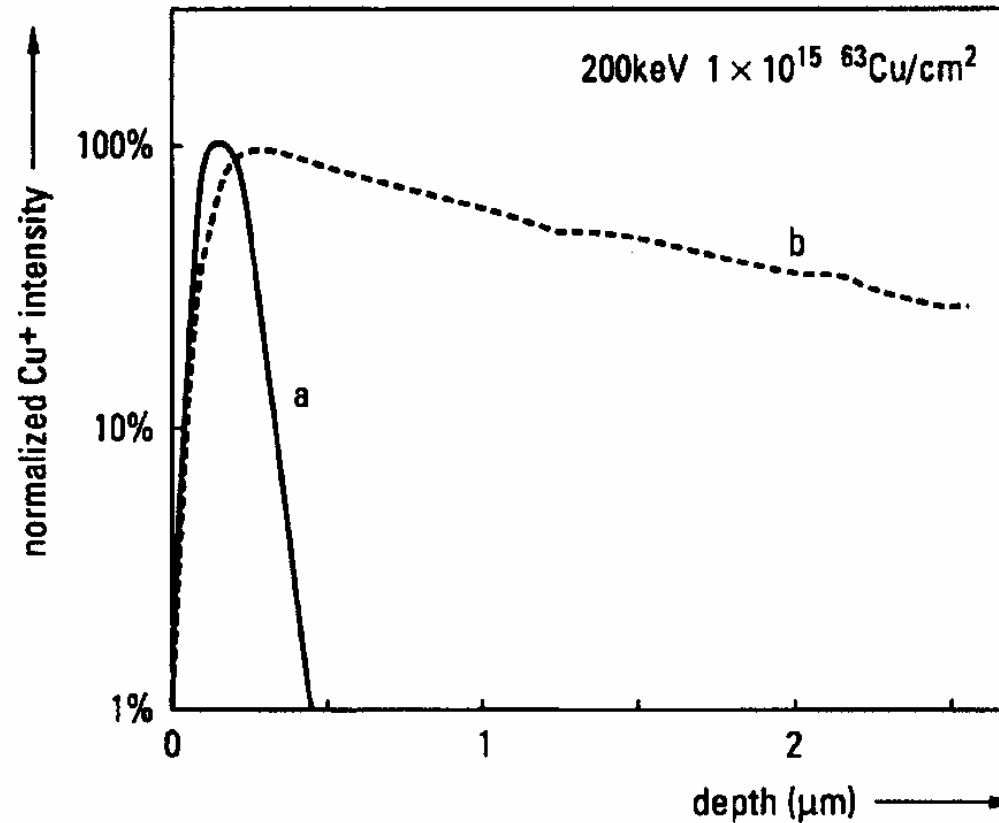
Statische SIMS mit ausreichend kleinem Primärstrom, während einer Messung wird weniger als 1 % der Oberflächenlage abgetragen, sonst dynamische SIMS



Positive secondary ion mass spectrum for silicon bombarded with oxygen ions. The inset shows a detailed scan around mass 31 in the high resolution mode ($M/\Delta M \sim 5000$); in the standard mode the various contributing moieties could never be resolved.



Ge depth distribution of a 25 nm Si / 30 nm Si_{0.75}Ge_{0.25} / Si-substrate structure as determined with a Cameca ims 4f using O₂ primary ions at various energies. Thin full line; E_p = 1.5 keV, β_p ~ 75°; thin dashed: 2 keV, ~ 60°; thin dotted: 3 keV, ~ 50°; thick drawn: 5.5 keV, 42°.

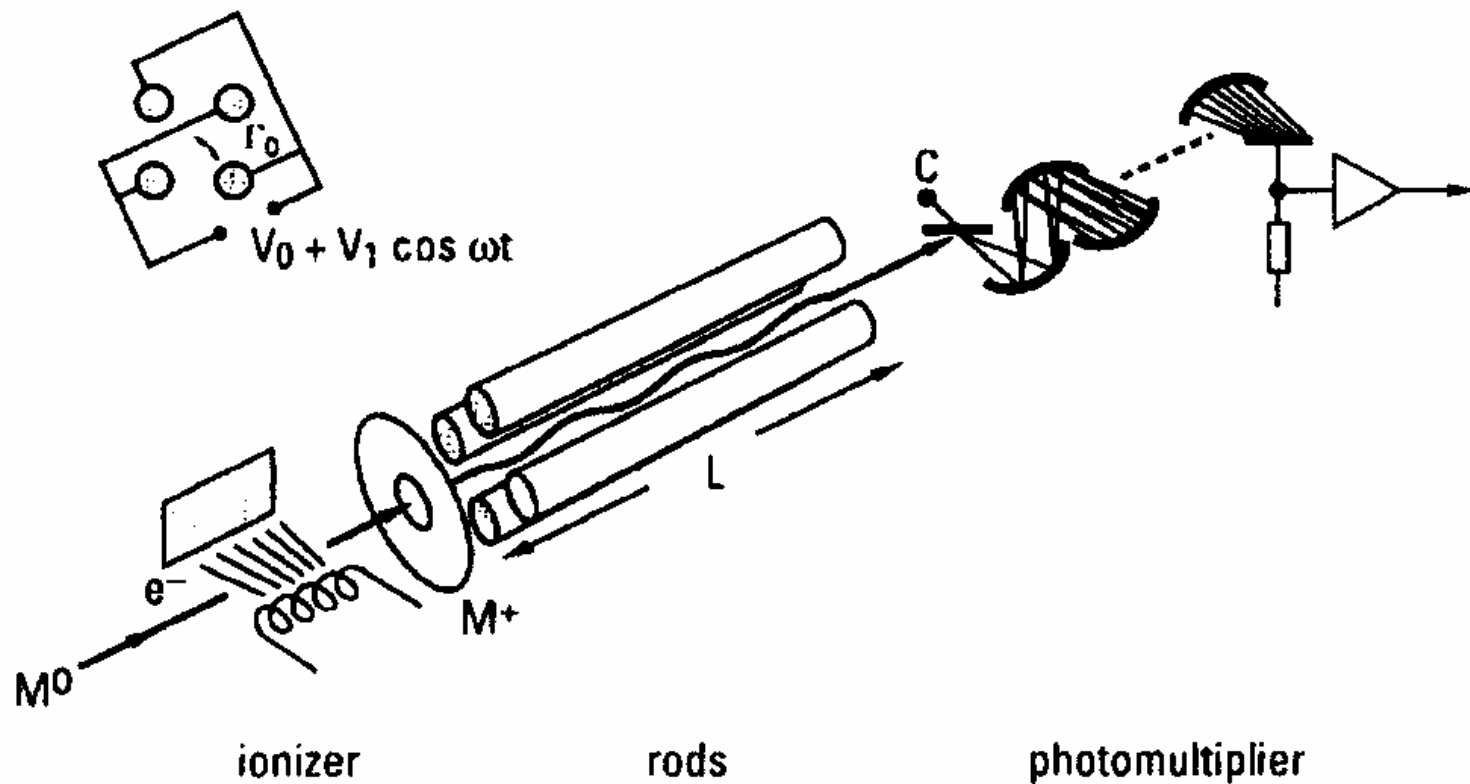


Depth profile of a copper implantation in silicon measured using O_2^+ primary ions incident at 45° off-normal such that the surface is not fully oxidized (a) and at perpendicular incidence where an SiO_2 layer forms (b). This demonstrates the dramatic effect of (local) sample charging leading to a redistribution over microns. Note that the signal intensity is normalized at the peak; in reality the segregating species gives an order of magnitude lower count rate.



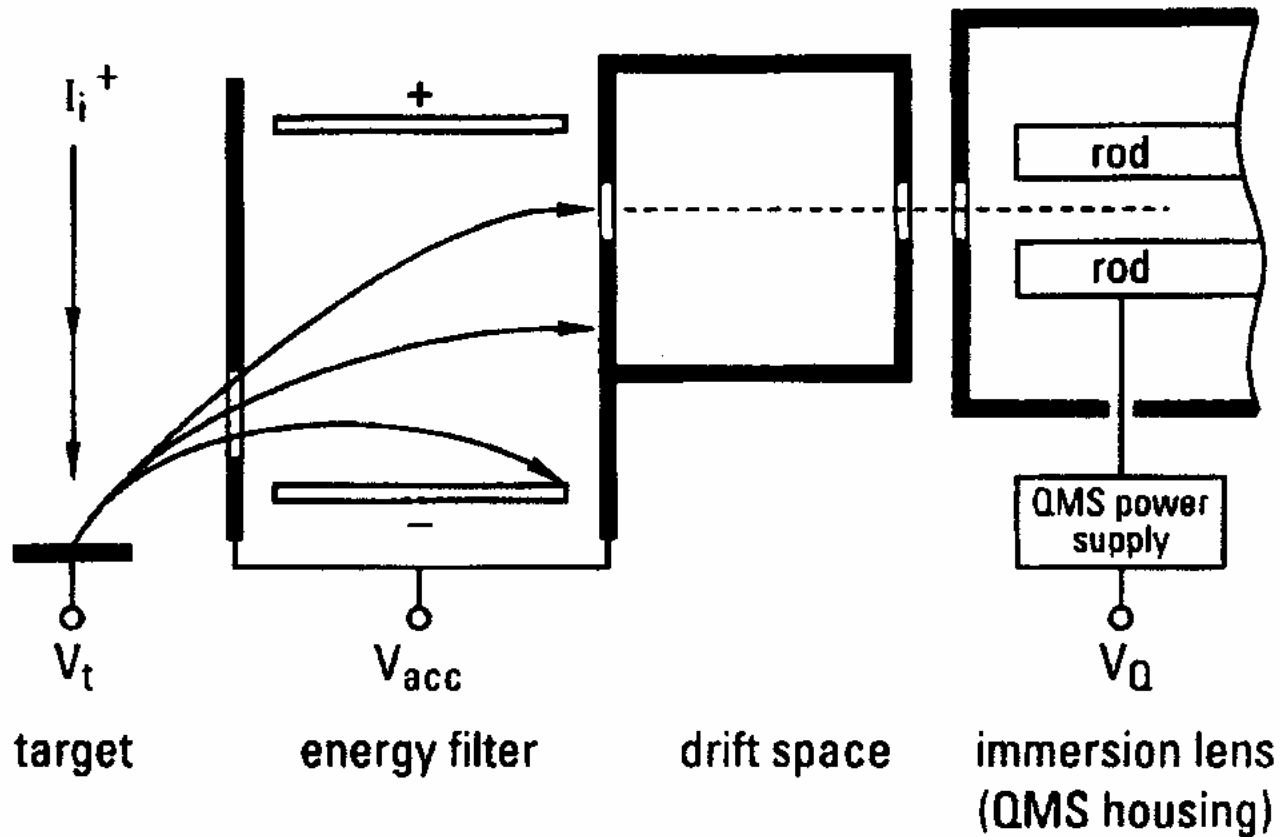
Any SIMS machine can be described as a combination of the following elements :

- (a) one (or more) primary ion source(s) ;**
- (b) a primary beam selector (more precisely, a purifying energy and/or mass filter) ;**
- (c) focus and deflection stage(s) ;**
- (d) target chamber with loadlock and holder ;**
- (e) a secondary ion energy discriminator ;**
- (f) the mass analyser ;**
- (g) the detector (assembly) ;**
- (h) data storage and manipulation facilities.**

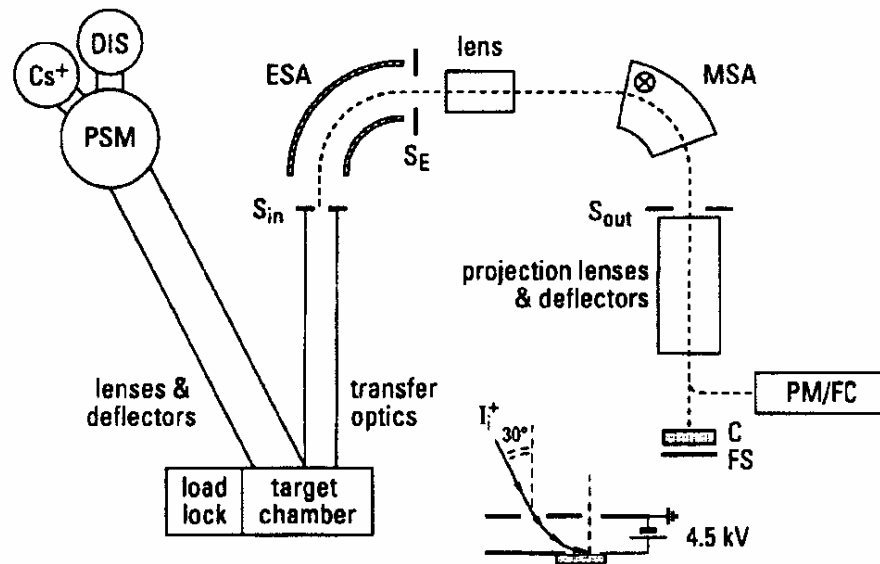


Working principle of a quadrupole mass filter (here used as a residual gas analyser). For particular values of V_0 , V_1 and ions with a specific mass-to-charge ratio pass between the rods on a stable oscillating path.

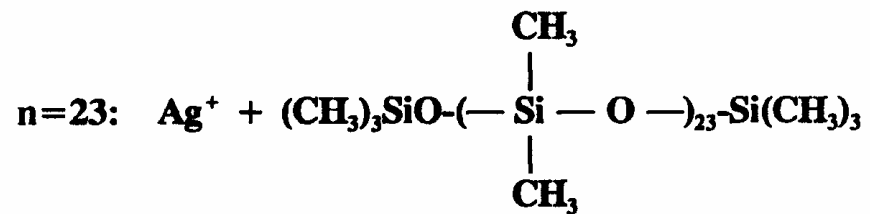
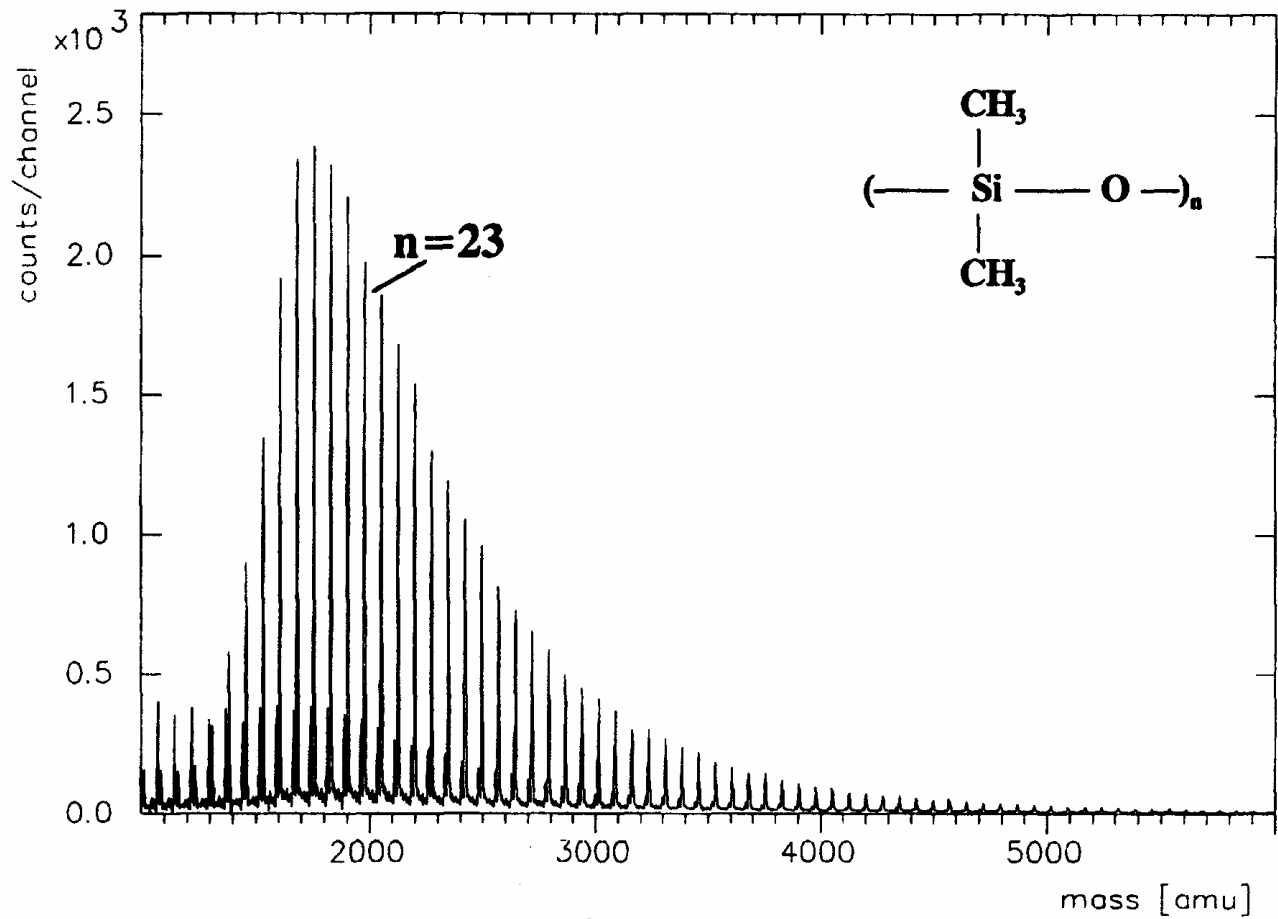


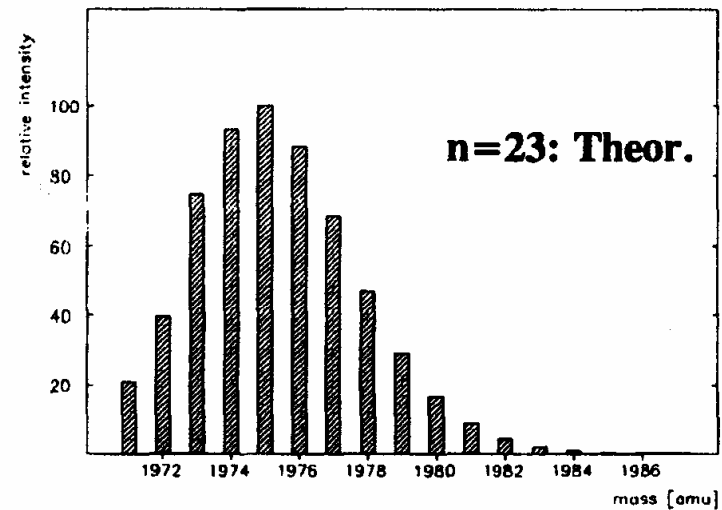
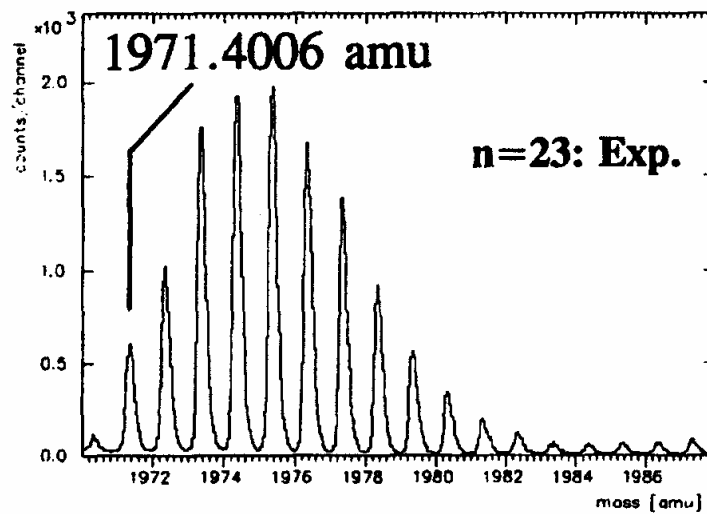


Extraction geometry of the Atomica ADIDA 2000 (see ref 25). The target may be biased (V_t) and secondary ions (here positive) are accelerated ($V_{acc} \sim 100\text{--}200\text{ V}$) toward the (parallel plate capacitor) analyser. After traversing the drift space they are retarded by the immersion lens prior to entering the quadrupole mass filter (which may be independently floating at V_Q).



Principle of the Cameca ims 3/4/5f secondary ion microscope/spectrometer. Ions from either a Cs^+ or a duoplasmatron ion source (DIS) pass, after extraction, a primary selection magnet (PSM) and are focused and rastered onto the sample. The secondary ions are accelerated away from the 4.5 kV biased target towards the grounded immersion lens which is part of the secondary ion transfer optics to enter the electrostatic sector analyser (ESA) through an entrance slit (S_{in}). The ESA is powered such that ions with the nominal energy of 4.5 keV are deflected over 90° . After passing the energy slit (S_E), which defines the transmitted part of the ejected kinetic energy spectrum, the secondaries are focused into the magnetic sector analyser (MSA). Mass resolution is defined by the exit slit (S_{out}) width. Finally deflection and projection into the detectors, either a photomultiplier (PM) or a Faraday cup (FC), or onto a channel plate fluorescent screen (C/FS) takes place. The insert shows, not to scale, the secondary ion extraction/primary beam retardation/target holder assembly for the particular combination of positive primary and secondary ions.





Positive ion mass spectrum of a monolayer of polydimethylsiloxane adsorbed onto an Ag film evaporated onto Si. Below the part around $M/e = 1971$ is expanded to show the agreement between observed (Exp.) and calculated (Theor.) isotope ratio for the peaks due to the particular neutral polymer molecules with $n = 23$ clustered to Ag^+ ions. Data courtesy of Dr H van der Wel, Phillips Research Laboratory, Eindhoven, The Netherlands.



5.2. Thermodesorptions-MS, Laserdesorptions-MS

Desorption adsorbierter Teilchen durch Wärmeeinwirkung (z.B. rückseitige Erwärmung mit Licht einer Xenonlampe (bei Vorderseite Photoeffekte zu befürchten), Analyse der Teilchen mit Quadrupolmassenspektrometer

Alternativ: Erwärmung mit Laserlicht, dabei wiederum bei frontseitiger Beleuchtung Photochemie denkbar



6. Elektronenstrahlmikroanalyse

EMPA: Electron microprobe analysis

EMP: Electron microprobe

EPMA: Electron probe microanalysis

EPXMA: Electron probe X-ray microanalysis

Verwandte Techniken:

SEM: Scanning electron microscope

(REM: Rasterelektronenmikroskop)

Auflösung: besser als 10 nm

Analytische Elektronenmikroskopie

Protoneninduzierte Röntgenemission PIXE

Röntgenfluoreszenzanalyse XRF

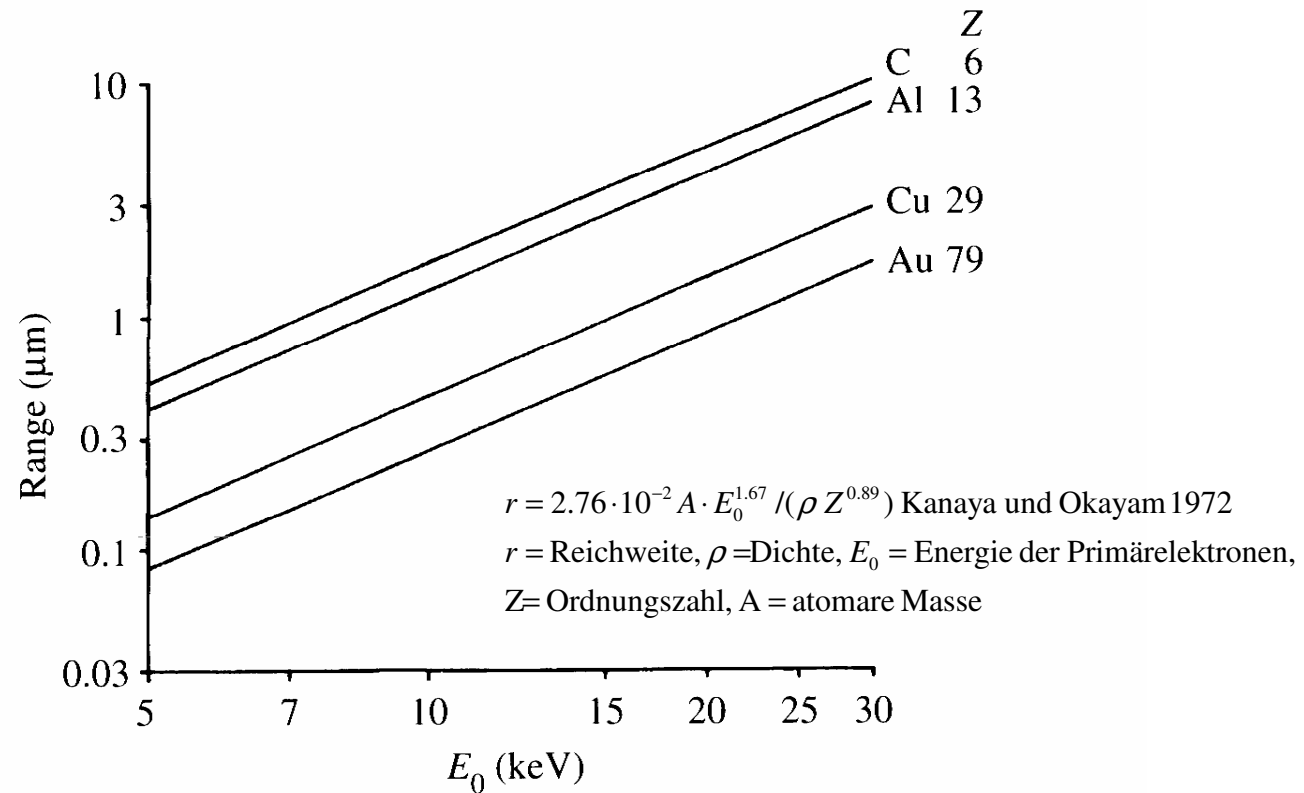
Auger-Analyse

Ion microprobe analysis (ähnlich SIMS)

Laserinduzierte Massenspektroskopie LIMS



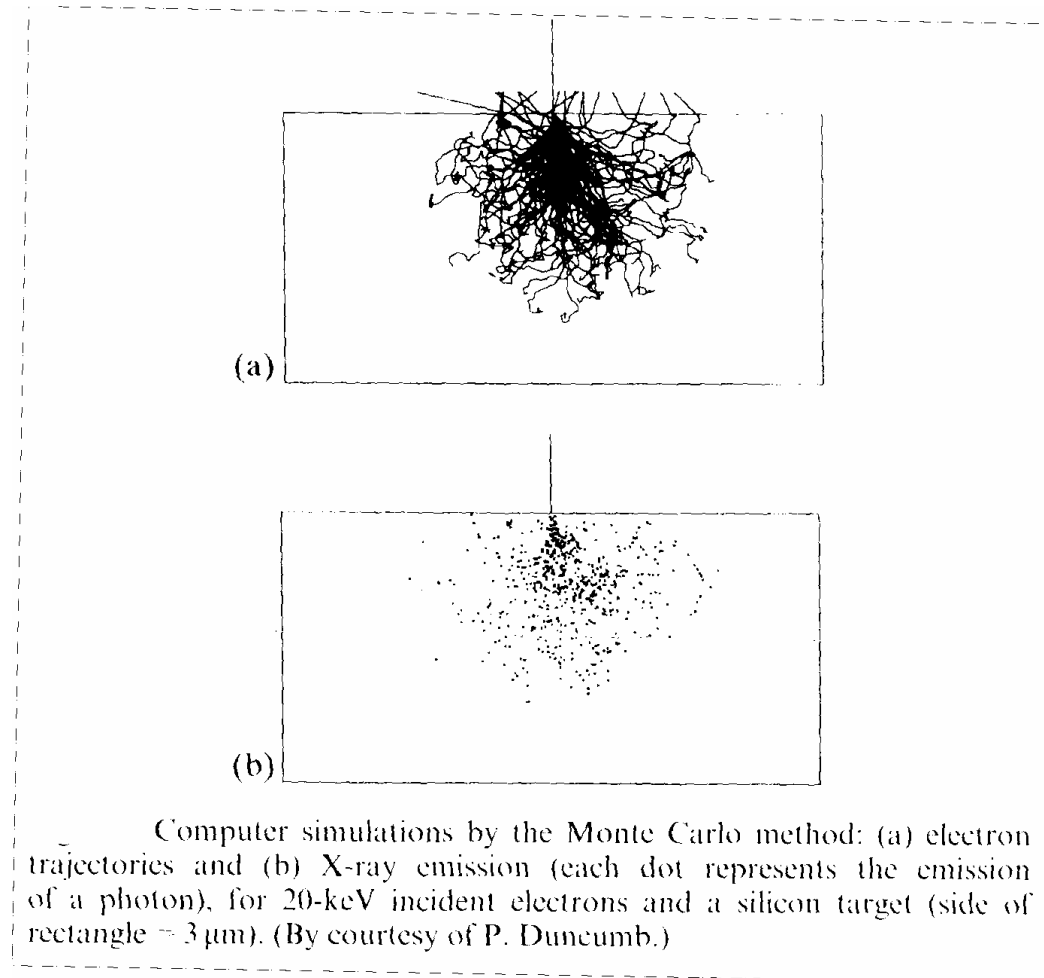
Inelastische Streuung von (Primär)Elektronen mit 5 .. 30 keV



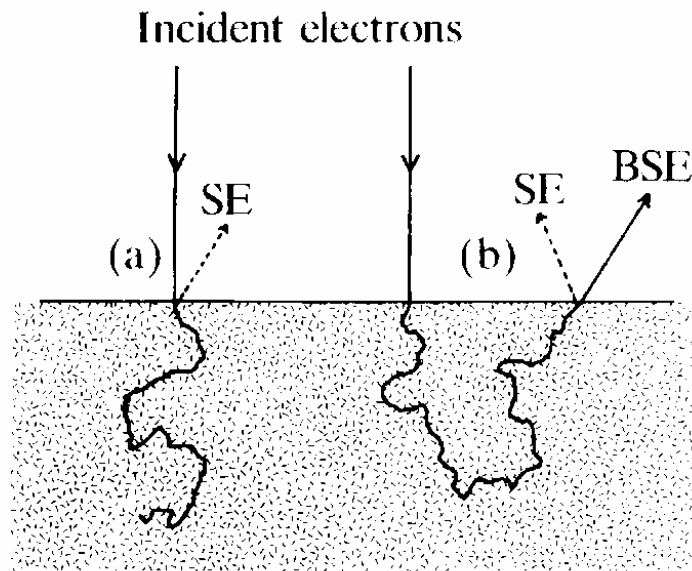
Electron range (defined as the mean straight-line distance from start to finish of electron trajectory in the target) as a function of incident electron energy (E_0) for target elements of various atomic numbers, calculated from the expression of Kanaya and Okayama (1972).



Elastische Streuung



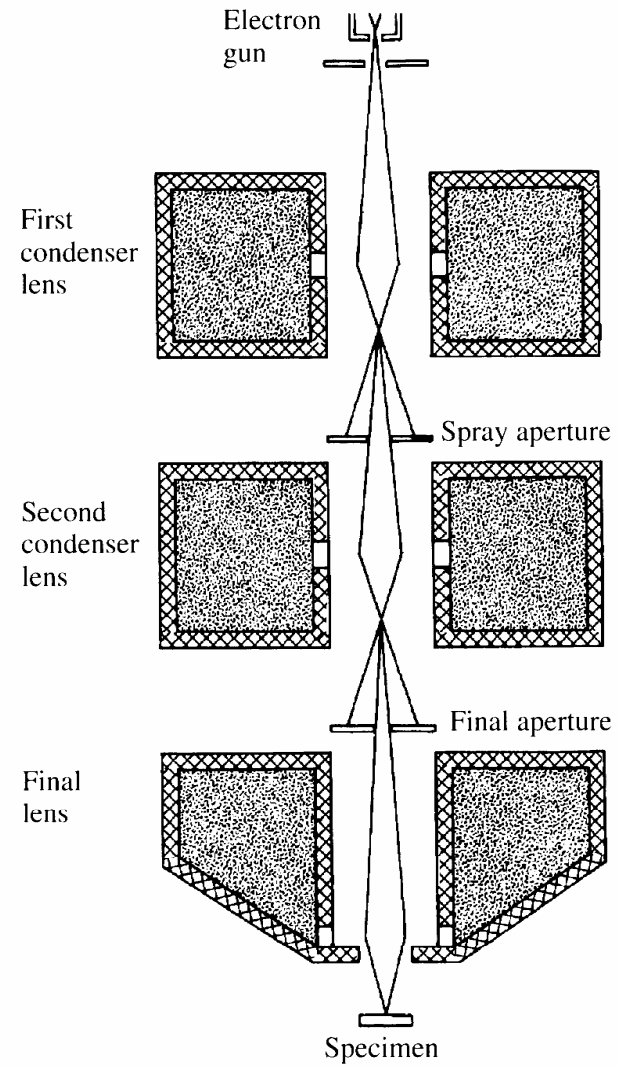
Quellen von Sekundärelektronen SE



Production of secondary electrons (SE): (a) by incident electrons entering target; and (b) by backscattered electrons (BSE) as they leave.

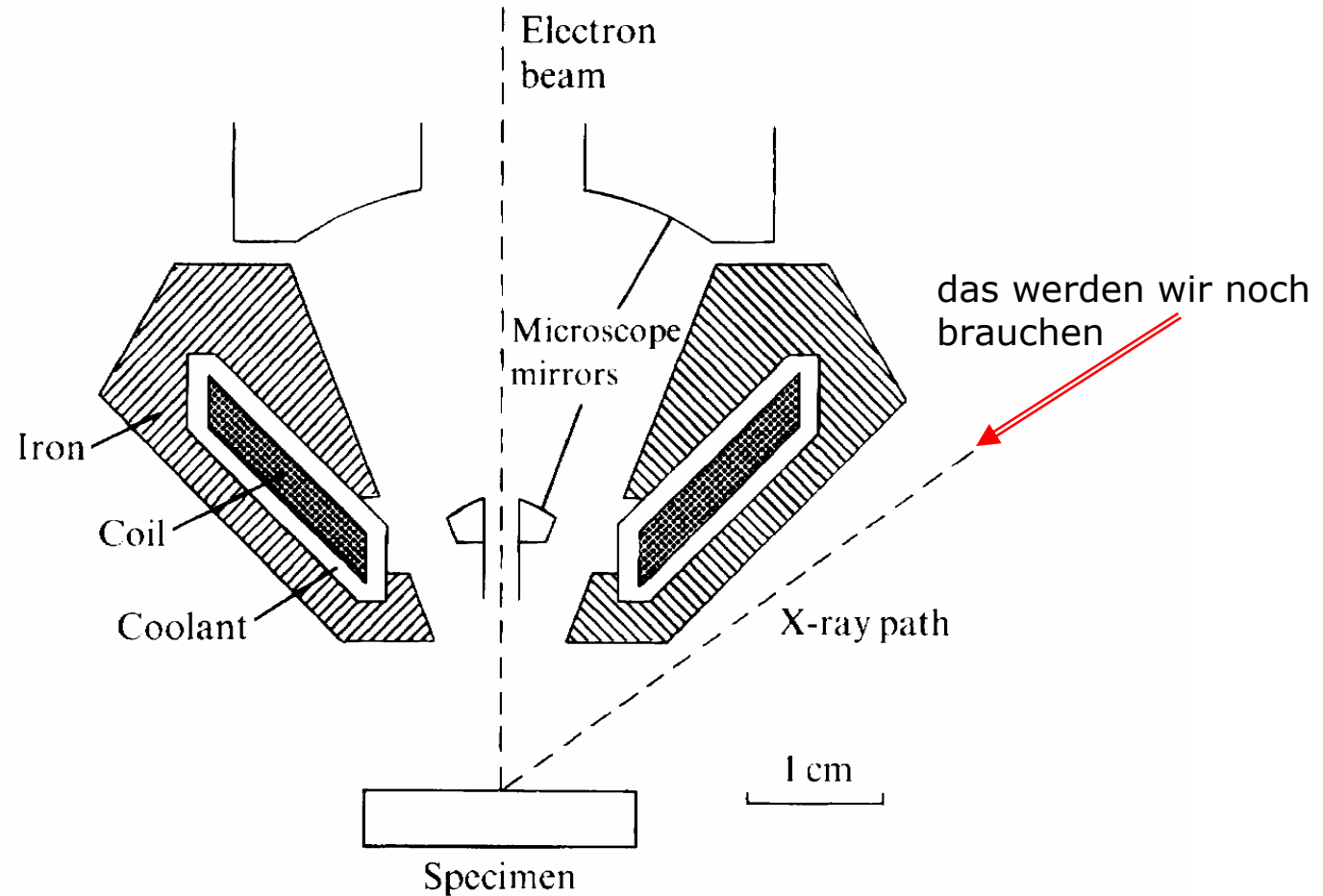


Das Instrument

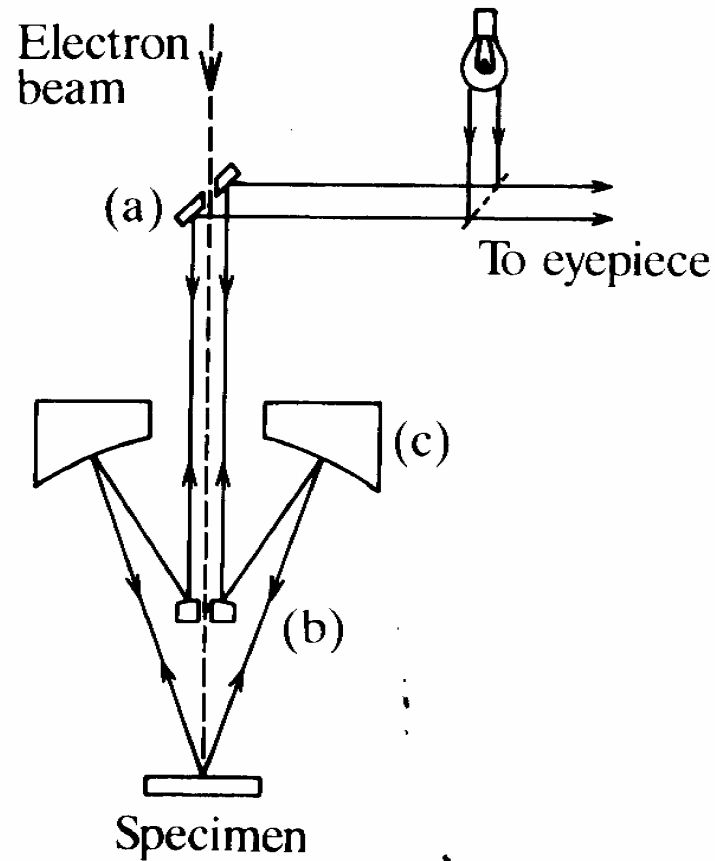


Schematic diagram of a three-lens probe-forming column as used in SEMs etc.: lenses produce a demagnified image of the electron source; aperture diaphragms intercept the unwanted part of the beam.

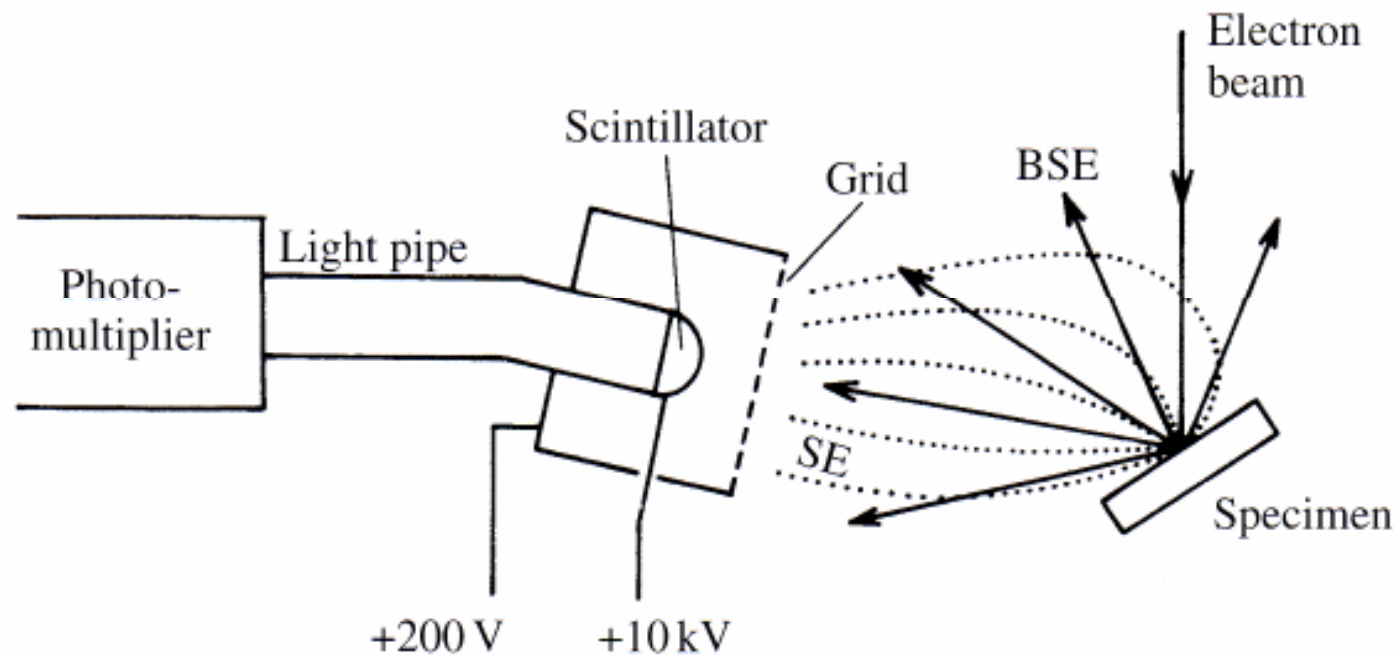




Final lens design for an electron microprobe (by courtesy of JEOL Ltd): liquid-cooled miniature lens allows space for optical microscope components and X-ray paths to spectrometers.



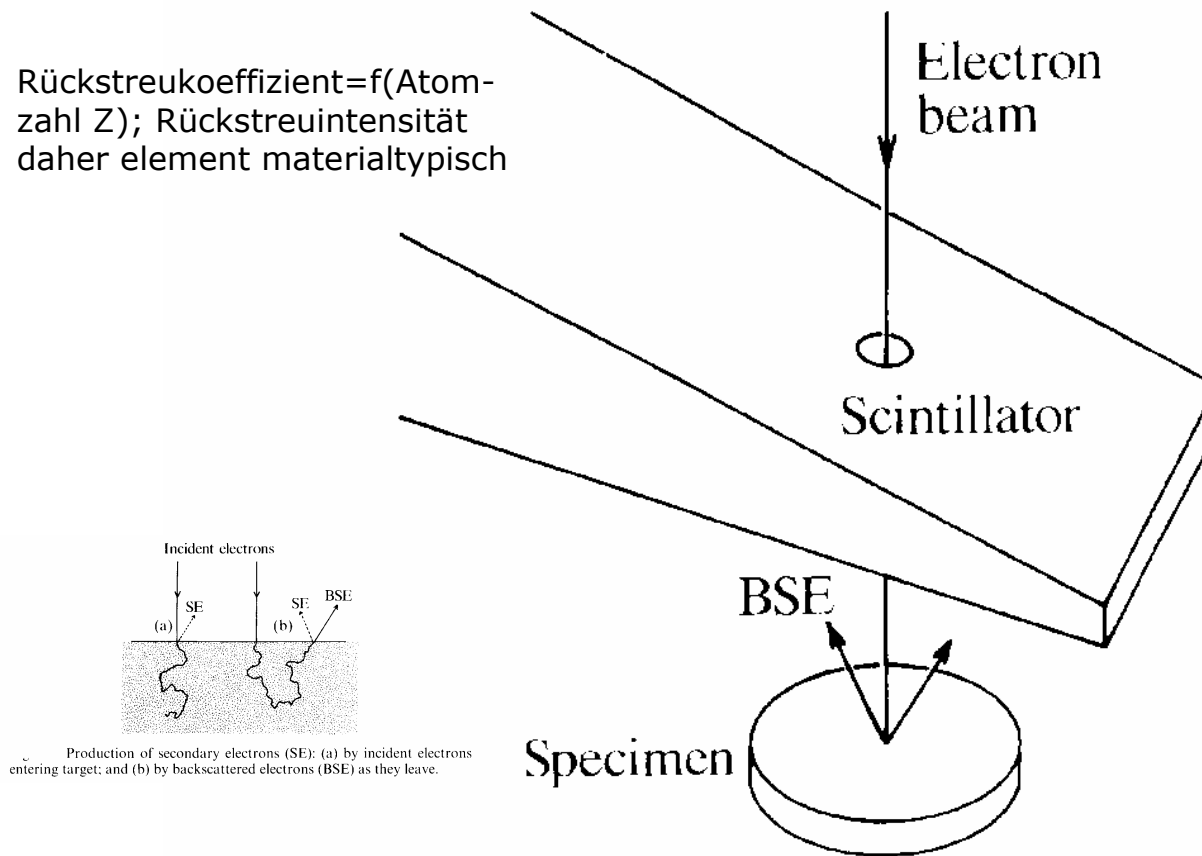
Reflecting microscope mounted coaxially with the electron beam, as fitted to electron microprobe instruments.



Everhart–Thornley detector, as used in SEMs: low-energy secondary electrons (SE) are attracted by +200 V on the grid and accelerated onto the scintillator by +10 kV; light produced by the scintillator passes along a transparent ‘light pipe’ to an external photomultiplier, which converts light into an electrical signal; backscattered electrons (BSE) are also detected, but less efficiently because they have higher energy and are not significantly deflected by the grid potential.



Rückstreukoeffizient = $f(\text{Atomzahl } Z)$; Rückstreuintensität daher element materialtypisch



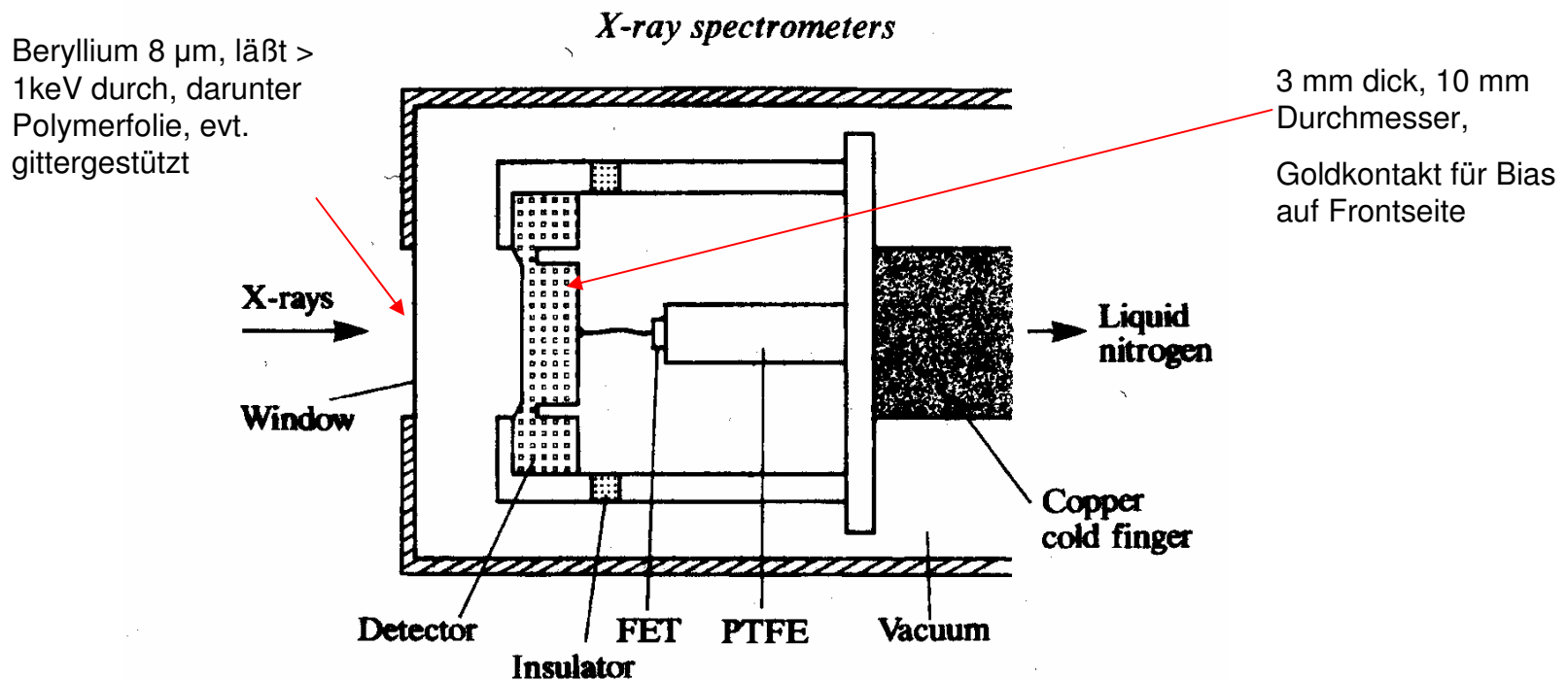
Backscattered-electron scintillation (Robinson) detector.

Mit negativer Gitterspannung am E-T-Detektor (Bild vorher) werden relativ energiearme Sekundärelektronen zurückgehalten, rückgestreute Elektronen kommen dagegen durch

Bei EMPA werden erzeugte Röntgenstrahlen ausgewertet:

- Energiedispersiv (ED)
- Wellenlängendispersiv (WD)

(daher für leichte Elemente weniger geeignet)



Mounting arrangements for a solid-state detector used for energy-dispersive spectrometry.

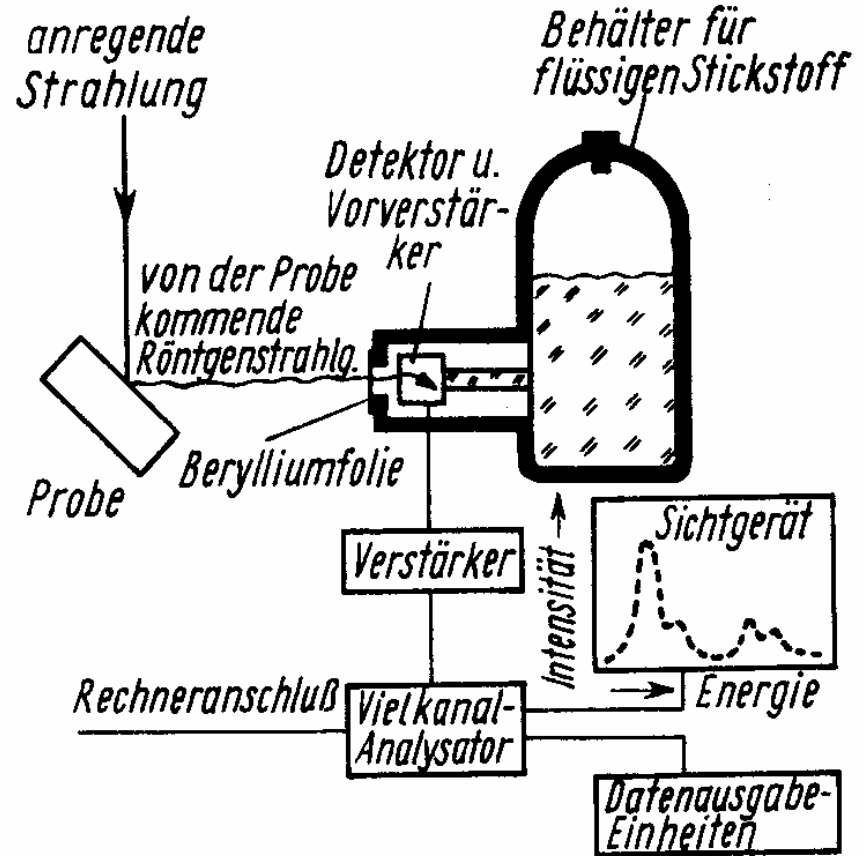
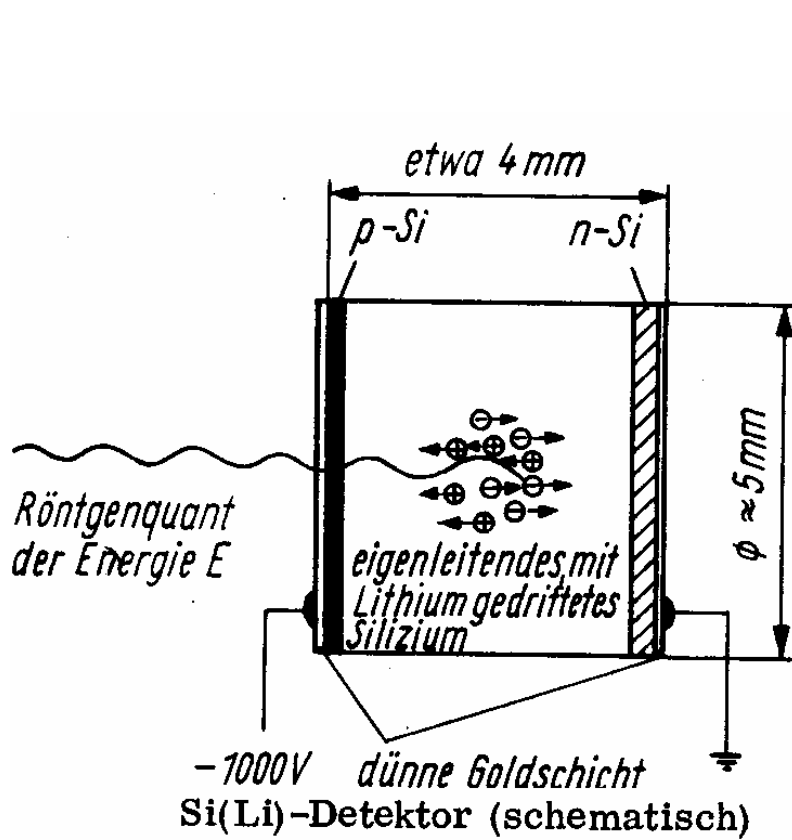


Wirkungsweise eines Detektors für energiedispersive Untersuchung:

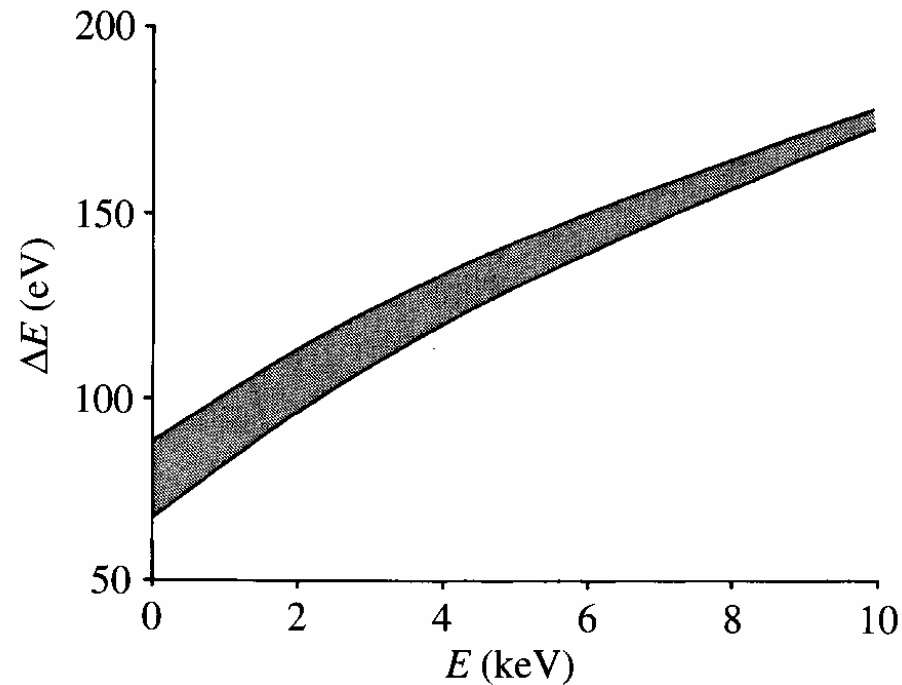
Auftreffendes Röntgenphoton löst im Halbleiter (Ge oder Si) Auger- und Photoelektronen aus, diese regen Elektronen aus dem Leitungs- ins Valenzband an, die am Halbleiter angelegte Vorspannung (Bias) läßt einen Stromimpuls entstehen, der hochohmig mit einem FET abgenommen wird.

Durchschnittsenergie zur Erzeugung eines Elektron-Loch-Paars für Si: 3,8 eV, für Ge 2,9 eV. Die Höhe des Stromimpulses hängt von der Zahl der erzeugten Paare ab, diese hängt von der Energie des Röntgenphotons dividiert durch die Paarerzeugungsenergie ab. Ein Al $K\alpha$ -Photon mit 1,487 keV erzeugt durchschnittlich 391 Paare in Si, ein Ni $K\alpha$ -Photon mit 7,477 keV dagegen 1970. D.h. Strom ist energieproportional – und damit elementtypisch.

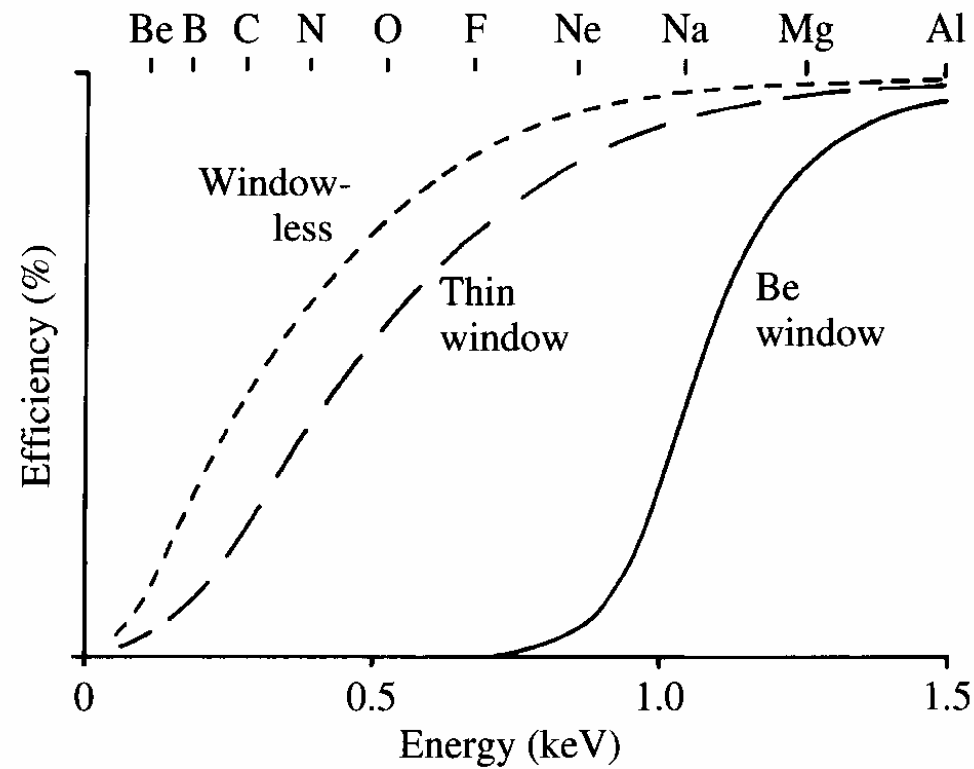
Verunreinigungen im Si werden durch Einbau von Lithium durch „driften“ kompensiert (Si(Li) lithium-drifted Si), Ge braucht dies nicht.



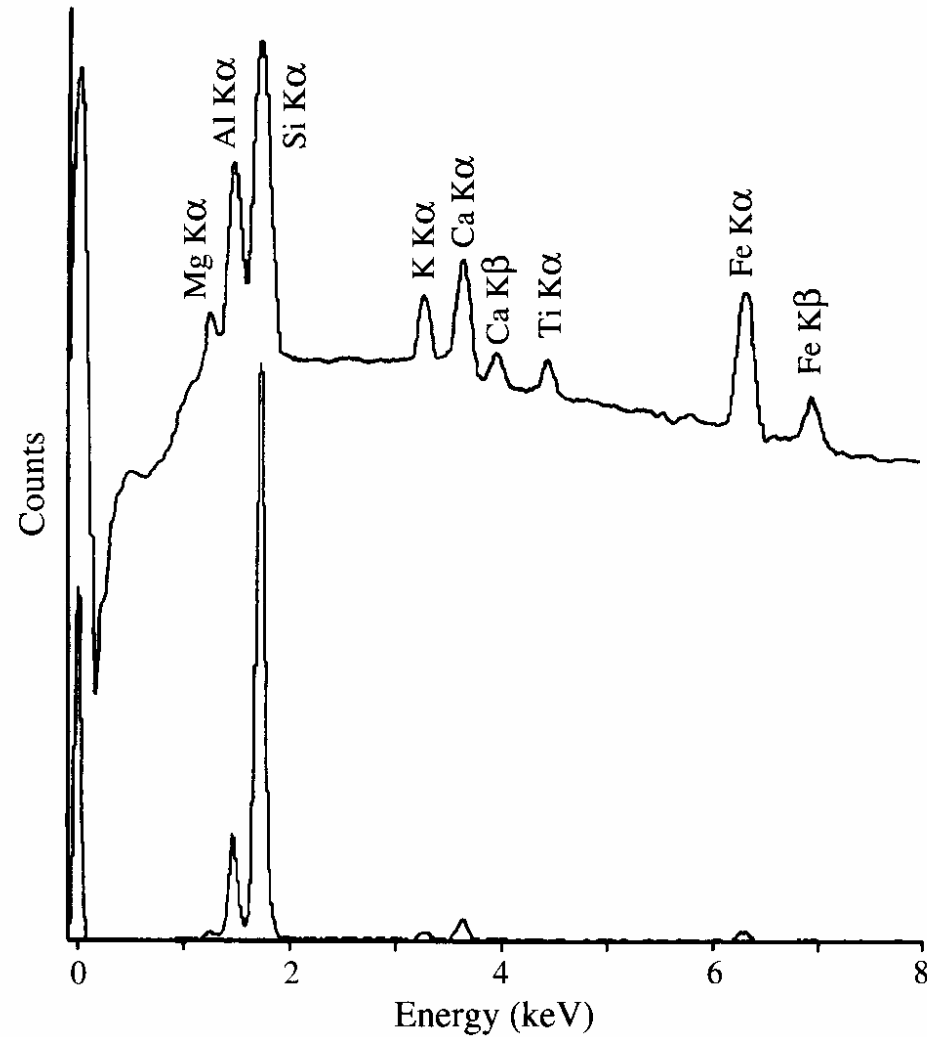
Prinzipieller Aufbau des energie-dispersiven Spektrometers



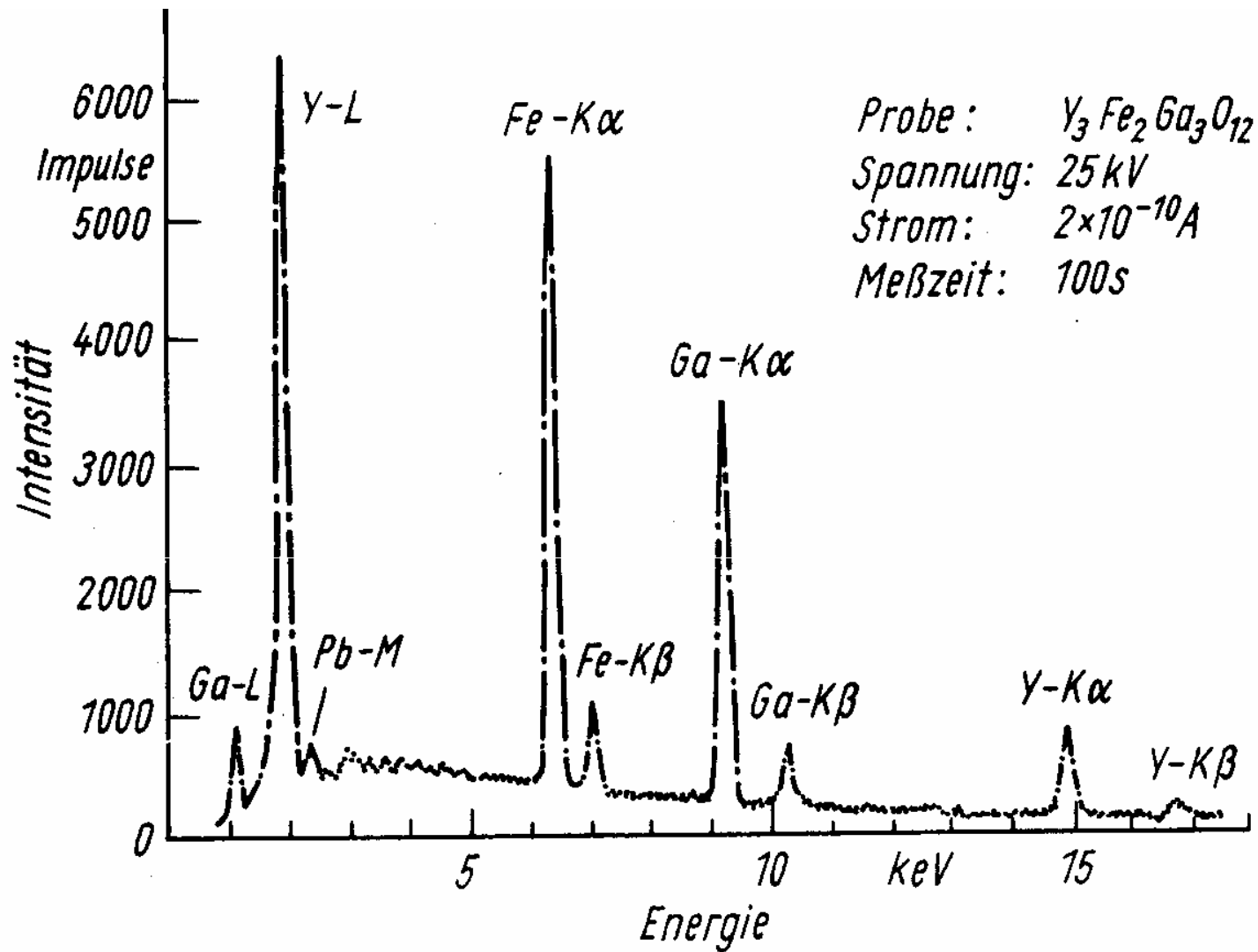
The energy resolution of an ED spectrometer as a function of the X-ray energy (E): ΔE is the full width at half maximum of the peak (see Fig. 5.2); the shaded area represents the range of values obtained with Si(Li) detectors.



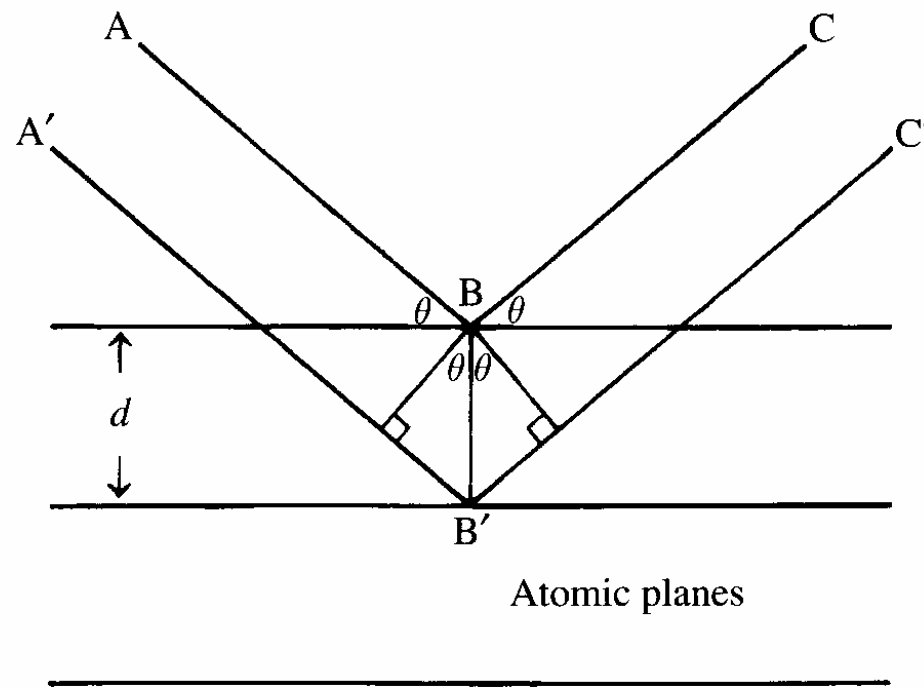
ED detector efficiency in the low-energy region, with various entrance windows (schematic only; the exact shape of the curve depends on window thickness and composition).



The energy-dispersive X-ray spectrum of a silicate mineral, consisting of a histogram of counts per channel, using logarithmic and linear scales (upper and lower curves, respectively).



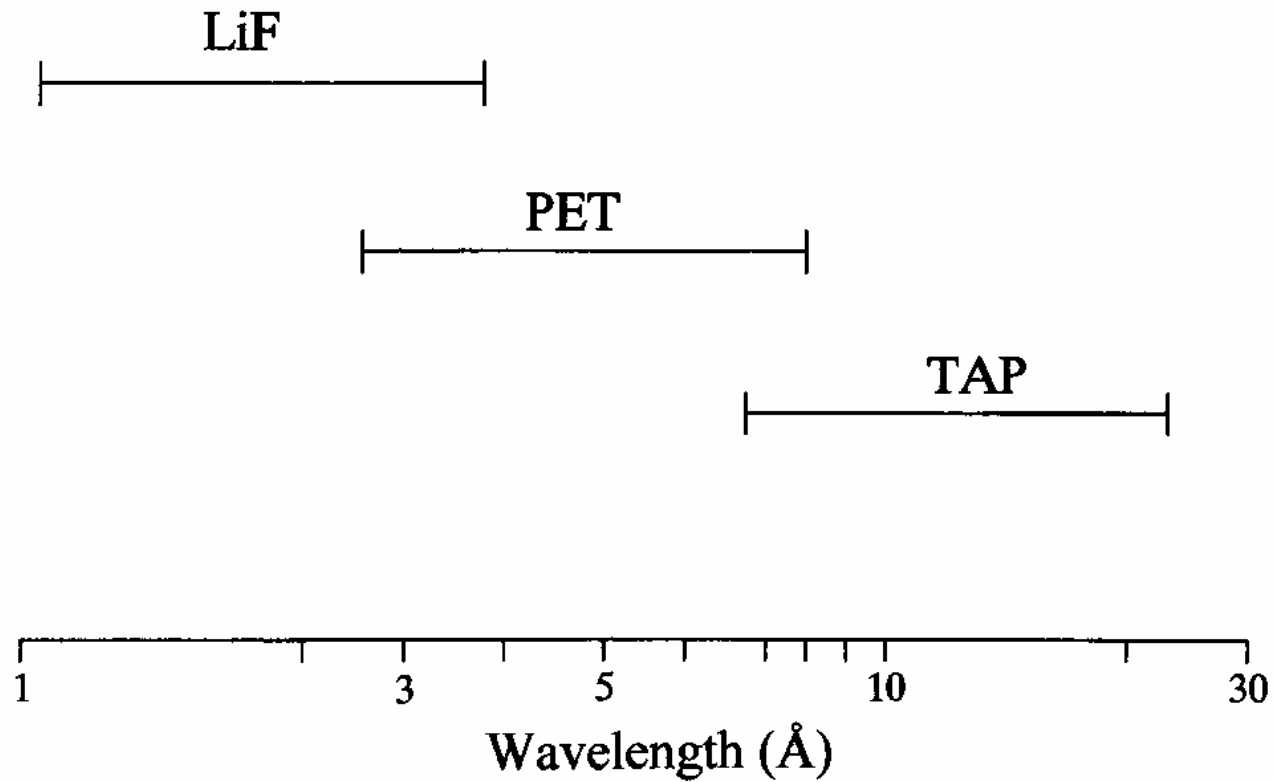
EDS-Spektrum eines Yttrium-Eisen-Gallium-Granat-Einkristalles



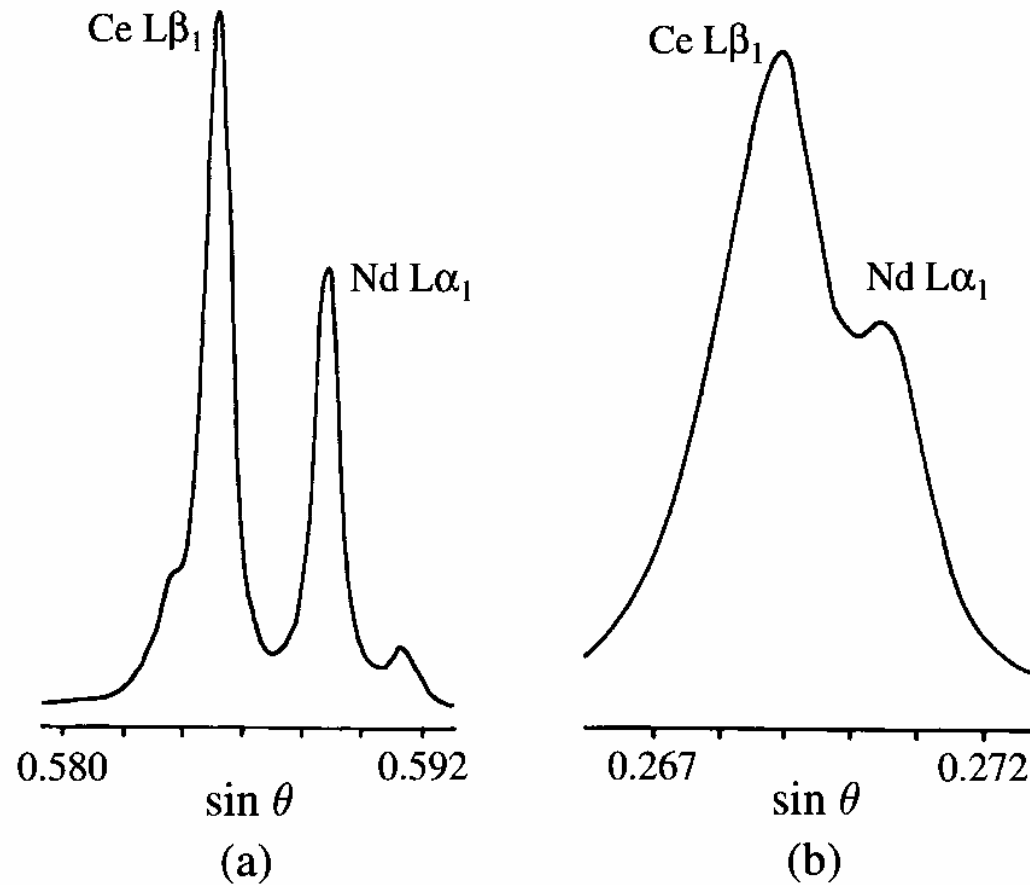
Bragg reflection: diffracted rays are in phase when distance $A' B' C'$ differs from $\bar{A} \bar{B} \bar{C}$ by an integral number of wavelengths.



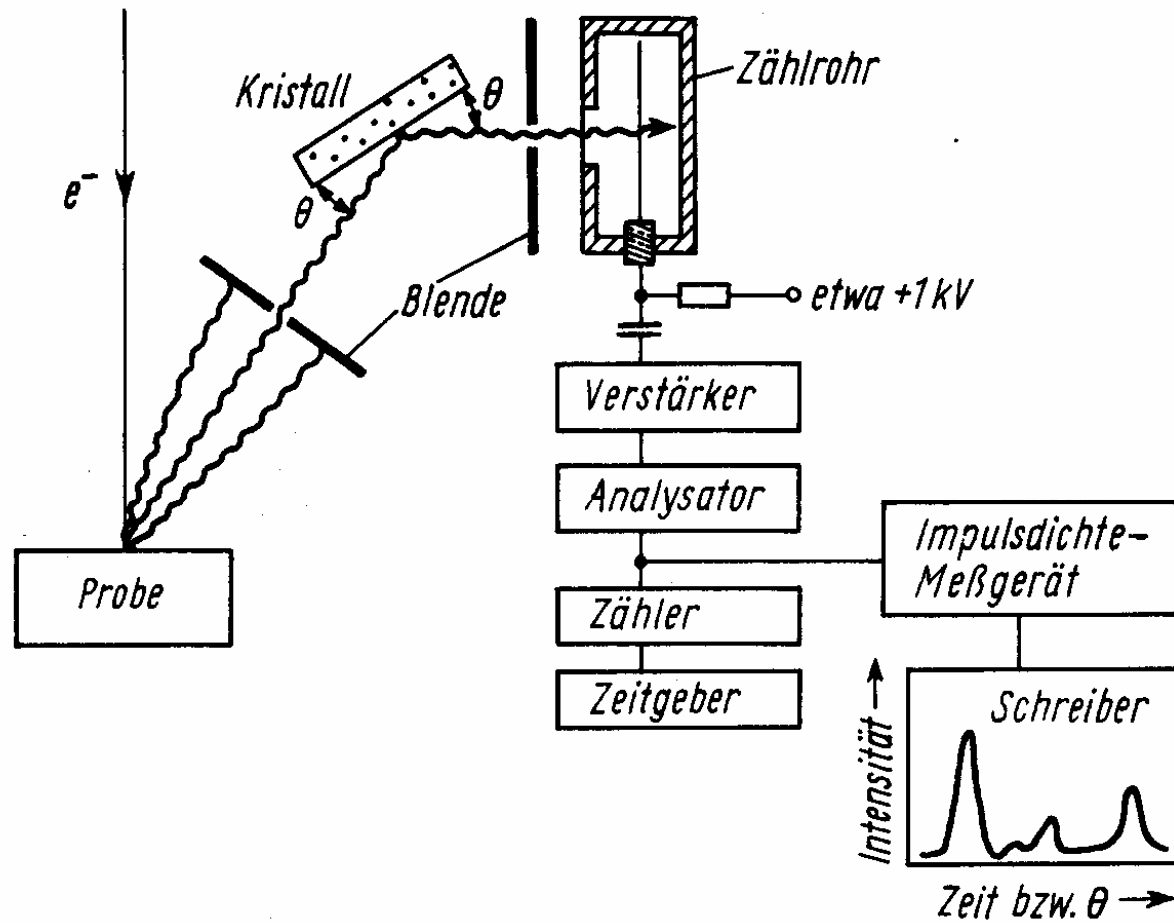
Kristall	2 d-Werte der entsprechenden Netzebenen (Å)		Reflexionsvermögen	Wellenlängenbereich (Å)	erfaßbarer Elementbereich		
					K	L	M
Lithiumfluorid, LiF	(200)	4,027	+++	0,8... 3,6	19...39	49...92	
Quarz, SiO ₂	(1011)	6,686	++	1,2... 6	15...32	40...80	>80
Pentaerythrit (PET), C ₅ H ₁₂ O ₄	(002)	8,742	++++	1,5... 8	13...29	35...72	>72
Ammoniumdihydrogenphosphat (ADP), (NH ₄)H ₂ PO ₄	(101)	10,642	++	1,8... 9,5	12...27	33...66	>70
Glimmer-Muskovit, KAl ₂ [AlSi ₃ O ₁₀](OH, F) ₂	(002)	19,84	+	3,5...18	9...20	29...51	>52
Rubidiumphthalat (RAP), C ₈ H ₅ O ₄ Rb	(1010)	26,121	+++	5 ...24	8...16	23...43	48...85
Kaliumphthalat (KAP), C ₈ H ₅ O ₄ K	(1010)	26,632	++	5 ...24	8...16	23...43	48...85
Blei-Stearat, Pb(C ₁₈ H ₃₅ O ₂) ₂		100	+++	20 ...90	4... 8	16...24	29...50



Wavelength coverages of crystals used in WD spectrometers.



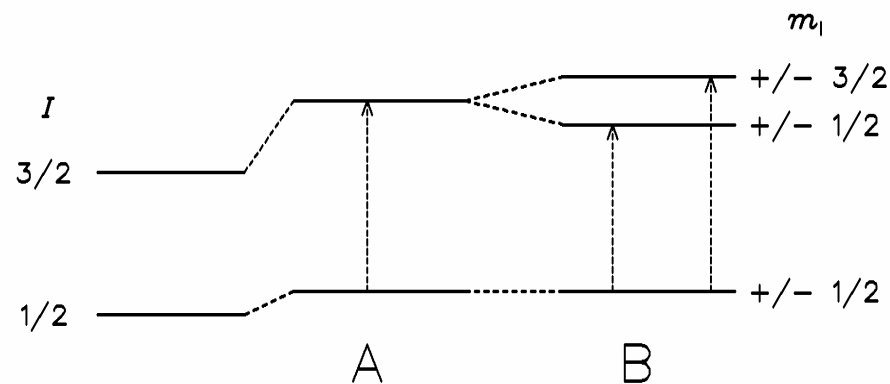
The effect of choice of crystal on resolution in a WD spectrum: peaks are resolved with LiF (a) but not with PET (b).



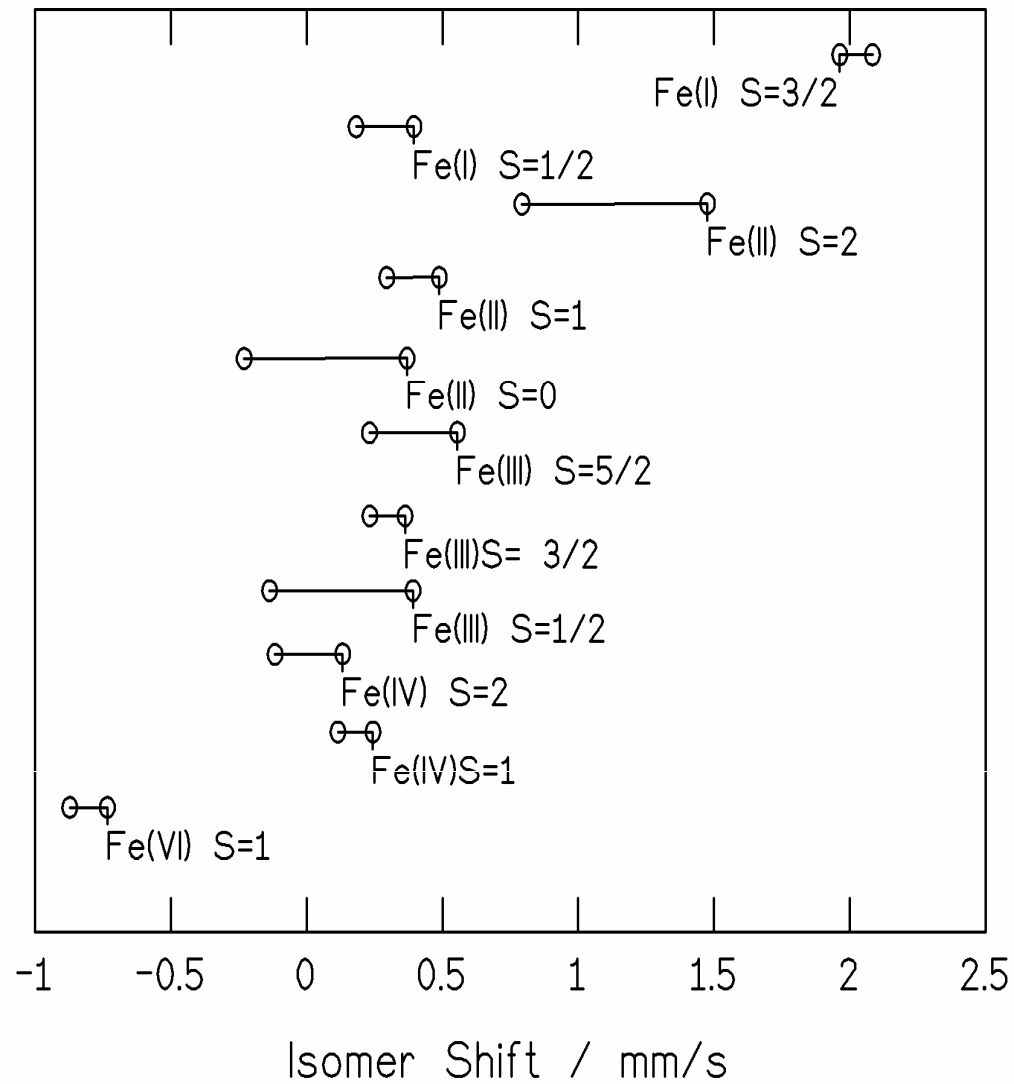
Prinzipieller Aufbau des wellenlängendispersiven Spektrometers

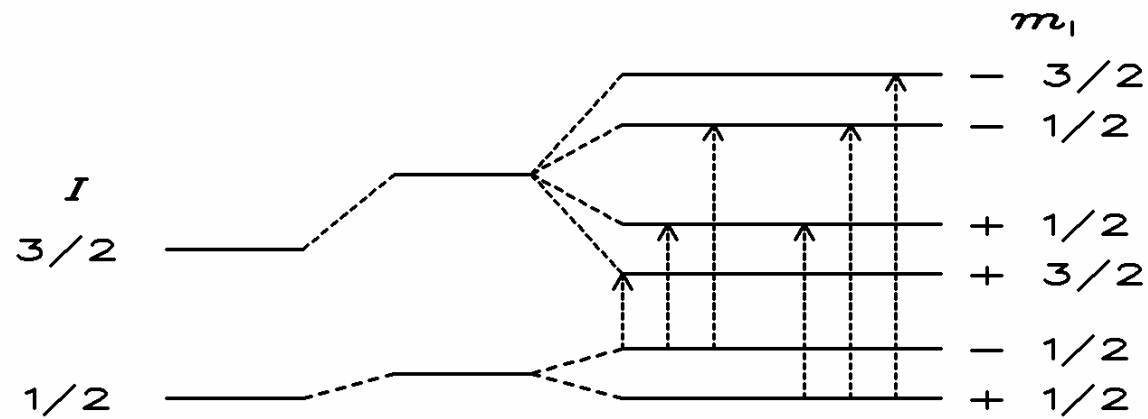


7. Mößbauerspektroskopie

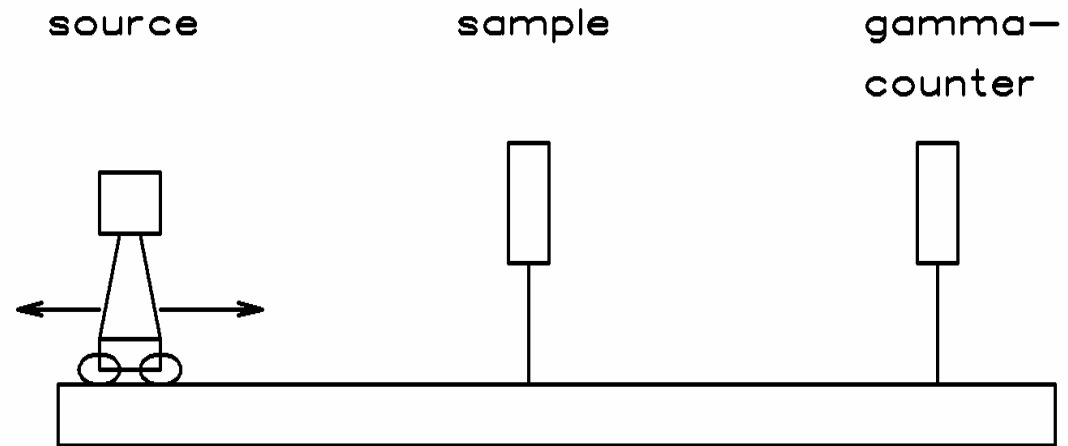


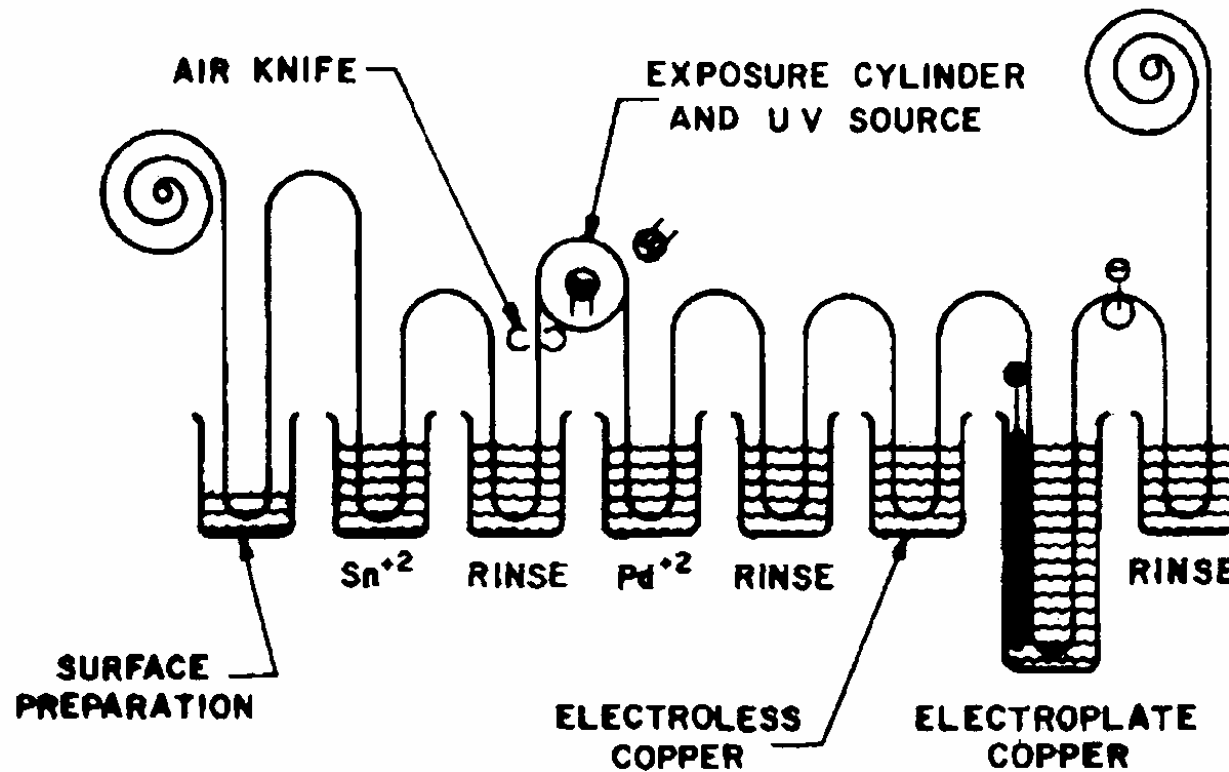
Isomerenshift A und Quadrupolsplitting B hängen von Elektronendichte am Kern, d.h. von z.B. Oxidationszahl, Bindungsverhältnisse (A) resp. von Symmetrie der Ladungsverteilung um den Kern (B) ab.





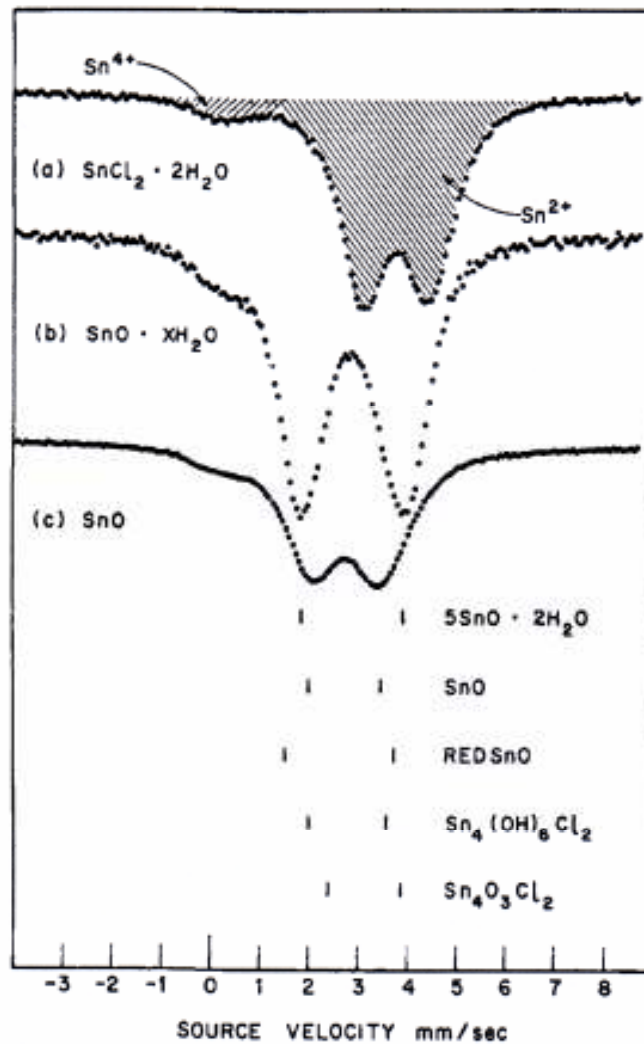
Magnetische Aufspaltung



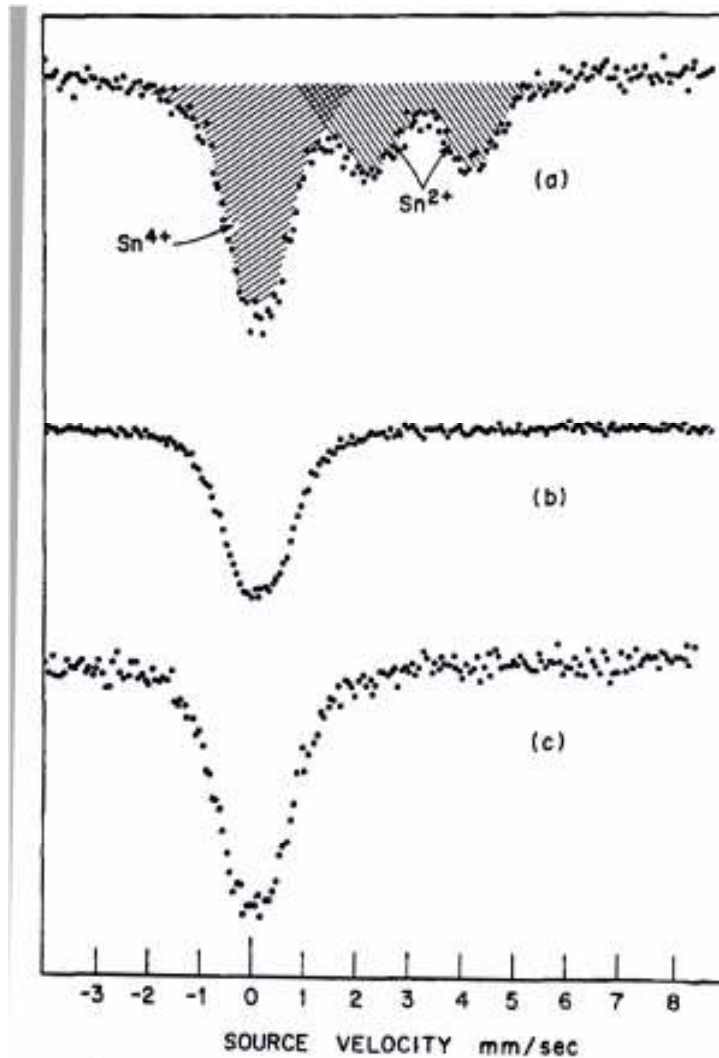


CONTINUOUS PHOTO PROCESSOR (SCHEMATIC)

Fig. 2. Outline of the various steps in the PSMD production process [from ref. (4)].



Observed spectra of three stannous compounds. The $\text{SnCl}_2 \cdot 2\text{H}_2\text{O}$ was Baker, reagent grade; the other two were made in our laboratory by standard preparative techniques. Note the existence of a line due to Sn^{4+} in all samples. Line positions reported in ref. (9) for various well-characterized tin compounds are shown below the spectra.



3. Spectra of the tin layers on Kapton foil: (a), sensitized by tin bath and unexposed; (b), sensitized by tin bath and uv exposed; (c), sensitized by tin bath and then dipped in Pd solution. The relative amounts of di- and tetravalent tin can be estimated (see footnote 1) from the relative areas in the corresponding spectral lines.



Literatur:

G. Ertl und J. Küppers: Low Energy Electrons and Surface Chemistry, VCH, Weinheim 1985

O. Brümmer: Mikroanalyse mit Elektronen- und Ionensonden, VEB Deutscher Verlag für Grundstoffindustrie, Leipzig, 1977

S.J.B. Reed: Electron Microprobe Analysis and Scanning Electron Microscopy in Geology, Cambridge University Press, Cambridge, 2005